Research Article

Journal of Applied Material Science & Engineering Research

Effect of Temperature and Magnetic Dopants on Particle size and Electrical Properties of ZnO Ceramic Varistor

A Sedky[1,2]*

[1]*Physics Department, Faculty of Science, Assiut University, Assiut, Egypt*

[2]*Physics Department, Faculty of Science, King Faisal University, Al-Hassa 31982, P.O.B 400, Saudi Arabia*

***Corresponding author**
A Sedky, Physics Department, Faculty of Science, Assiut University, Assiut, Egypt, Tel: 00201157803325 2; Fax: 002088234708; E-mail:sedky1960@yahoo.com

Submitted: 08 Mar 2018; **Accepted**: 17 Mar 2018; **Published**: 12 Apr 2018

Abstract

We report here structural and electrical properties of $Zn_{0.95}$ $M_{0.05}O$ ceramic, M = Zn, Co and Mn. It is found that addition of magnetic doping did not influence the hexagonal wurtzite structure of ZnO. Furthermore, the lattice parameters ratio c/a for hexagonal distortion and the length of the bond parallel u to the c axis were nearly unaffected. The average crystalline diameters, deduced from XRD analysis are 83.75, 72.86 and 70.97 nm for Zn, Mn and Co, which are 15 times lower than those obtained from FESEM micrographs (1570, 1380 and 1150 nm). The breakdown field EB was decreased as the temperature increased, in the following order: Mn> Zn > Co. The nonlinear region was observed for all samples as the temperature increased up to 400 K and completely disappeared with further increase of temperature up to 500 K. The values of nonlinear coefficient, α were between 1.65 and 56 for all samples, in the following order: Mn> Zn > Co. Moreover, the electrical conductivity σ was gradually increased as the temperature increased up to 500 K, in the following order: Co > Zn > Mn. On the other hand, the activation energies were 0.194, 0.155 eV and 0.231 eV for all samples, in the following order Mn, Zn and Co. These results have been discussed in terms of valence states, magnetic moment and thermo-ionic emission which were produced by the doping, and controlling the potential barrier of ZnO.

Keywords: Ceramics, Chemical synthesis, X-ray diffraction, Electrical properties

Introduction

The ZnO based ceramic semiconductors are widely used as gas sensors, piezoelectric transducers, electrode for solar cells and varistors [1-4]. This is because ZnO ceramics are multiphase device which exhibit highly nonlinear current- voltage characteristics due to its electrostatic potential barrier formed at grain boundaries [5-8]. However, a considerable numbers of studies have been carried out into the nonlinear behaviour obtained in the J-E characteristics of ZnO [9].

Normally, the ZnOvaristors are typically fabricated by sintering of ZnO with other metal oxides as additives. These additives are the main tools which are used to test the nonlinear response and also the stability of ZnOvaristor [10-16]. Several efforts have been carried out to describe the influence of additives, such as Bi_2O_3, Cr_2O_3, Al_2O_3 , MnO, CoO, and Fe_2O_3 on the microstructure and electrical properties of ZnO [8,11,14-20]. It is found that the nonlinear current-voltage characteristics of ZnOvaristors are directly dependent on the composition and microstructure, such as density, phase purity crystal structure and grain size. By controlling these parameters, the nonlinear coefficient and breakdown field of ZnOvaristors may be improved.

As one promising metal-oxide material in the semiconductor field due to its potential properties, ZnO is a wide band-gap material with an energy gap of 3.3 eV and the large exciton binding energy of 60 meV at room temperature [21]. The ZnO band structure and its optical properties are very similar to those of GaN, which helps for fabrication of ZnO in the optical device such as light emitting diodes (LEDs) and laser diodes (LDs).

It is well known that the nonlinear behaviour of pure ZnO may be unaffected by the temperature, and normally it is changed to linear behaviour as the temperature increases. This is reflected to increasing the thermo-ionic emission of ZnO by increasing the temperature. But with different magnetic additives, the answer remains unclear and may be not reported. With this purpose in this work a range of ZnO ceramic samples $Zn_{0.95}M_{0.05}O$ with different magnetic ions M = Co, Mn as additives are synthesized and tested for phase purity and structural morphology by XRD and SEM techniques.While the J-E characteristics are obtained by dc electrical measurements in the temperature range of (300 K -500 K). Furthermore, the electrical conductivity and activation energies are obtained and discussed for all samples.

Experimental Details

$Zn_{0.95}M_{0.05}O$ samples with M = Zn, Co, and Mn are synthesized by using conventional solid-state reaction method. The powders of

ZnO Co and Mn_2O_3 (Aldrich 99.999 purity) are thoroughly mixed in required proportions and calcined at 1000^0C in air for a period of 12 hours. The resulting powders are ground, mixed, and pressed into pellets of 1 cm diameter and 0. 35 cm thick. The pellets are then sintered at temperature of 1000^oC for 10 h in air, and then quenched down to room temperature. The bulk density of the samples is measured in terms of their weight and volume. The phase purity of the samples is examined by using X-ray diffractmeter with Cu-Kα radiation and field emission scanning electron microscope (FESEM). I-V characteristics are obtained by using dc electrical circuit with an electrometer (model 3 6517, Keithley), dc power supply (5 K v), temperature controller and digital multimeter. The samples are well polished and sandwiched between two cupper electrodes and the current is measured relative to the applied voltage at different values of temperatures (300 - 500 K). From the values of currents and voltage, the values of current density J and electric field E are obtained.

Results and Discussion

The bulk density of ZnO, listed in Table 1, is decreased by the doping. It is generally changed to 76 % for Co and to 90 % for Mn as compared to the density of ZnO. It is worthy to note that the bulk density for the doped samples contradicts with the behavior of lattice parameters discussed below. This might be due to increasing the number of pores which counterbalance the decrease of lattice parameters. Figure 1 shows X-ray diffraction patterns for the samples. It is evident from the Figure that the structure of all samples is Wurtzite structure, and the other reacted phases are not formed. The obtained peaks (100), (002), (111), (102), (110), (103), (200), (112), (201), (210) and (211) shown in the XRD patterns can be identified as the hexagonal wurtzite structure of ZnO ceramic.

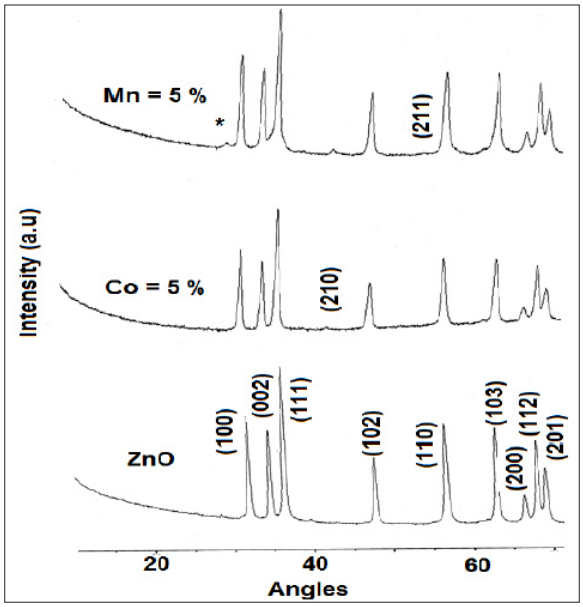

Figure 1: XRD patterns of $Zn_{0.95}M_{0.05}O$ samples

To further confirm that the doping have been substituted for Zn^{2+} in the unit cell, the lattice parameters are calculated and listed in Table 1. The decrease of lattice 4 parameters by the doping, probably due the smaller ionic size of doping (Co^{3+} = 0.63 Å, and $Mn^{3+/4+}$ = 0.63 Å) than that of Zn^{2+} (0.74 Ă). The lattice constants mostly range from 3.235 to 3.243 Å for the - parameter, and from 5.197 to 5.211 Å for the c - parameter. However, in a real ZnO crystal, the wurtzite structure usually deviates from the ideal arrangement by changing either the c/a ratio for hexagonal distortion or the u value which describing the length of the bond parallel to the c axis. In units of c, u is given by $u = 0.333\ (a/c)^2 + 0.25$ [22] (Kisi E et.al 1989), and it is equal 0.375 in an ideal wurtzite structure in fractional coordinates.

On the other hand, the average crystalline diameter D_{hkl} is evaluated in terms of X-ray line broadening described by the following Scherer's equation [22];

$$D_{hkl} = \frac{k\lambda}{\Delta\theta\cos\theta} \qquad (1)$$

Where λ is X-ray wavelength (λ = 1.5418 Ă), Δθ is half maximum line width, θ is Bragg angle and K is constant (K = 0.9 for this type of ceramics). It is clear from Table 1 that $D_{(111)}$ values of $D_{(111)}$ are between 83.74, 72.97 and 70.86 nm for Zn, Mn and Co, respectively.

Table 1 : Ea versus doping content for $Zn_{0.95}M_{0.05}O$ samples

doping	ρ (gm/cm³)	a (Å)	c (Å)	a/c	U	D_{XRD} (nm)	D_{SEM} (nm)	E_a (eV)
Zn	4.82	3.243	5.211	0.622	0.379	83.74	1570	0.194
Co	3.66	3.237	5.197	0.623	0.379	70.86	1150	0.155
Mn	4.35	3.235	5.201	0.622	0.379	72.97	1380	0.231

The c/a ratio and u value listed in Table 1 are nearly constant for all samples. It should be pointed out that a strong correlation may be exists for ideal wurtzite between the c/a ratio and u parameter in that when the c/a ratio decreases, the u parameter increases in such a way that those four tetrahedral distances remain nearly constant through a distortion of tetrahedral angles due to long-range polar interactions. However, the deviation from that of the ideal wurtzite structure is probably due to lattice stability and iconicity could not be obtained in the present case [23]. The microstructure of the samples is shown in Figure 2 (a-c). Although, no second phases are formed by the doping at the grain boundaries, the average grain size is decreased as compared to ZnO sample. The flake type grains are absent in all samples, and there is a uniform granular precipitation on the mother grains. The average grain size (D) is determined by the lineal intercept method with the help of the expression, $D = \frac{1.56L}{MN}$ Where L is the random line length on the micrograph, M is the magnification of the micrograph, and N is the number of the grain boundaries intercepted by the lines [24].

The average crystalline diameters are decreased from 1570 nm to 1380 nm and 1150 nm for Mn and Co samples, in the following the order Zn >Mn> Co.

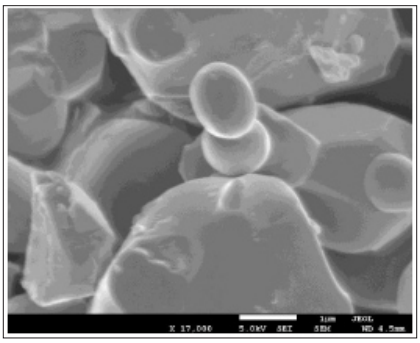

Figure 2 (a): SEM micrographs of ZnO sample

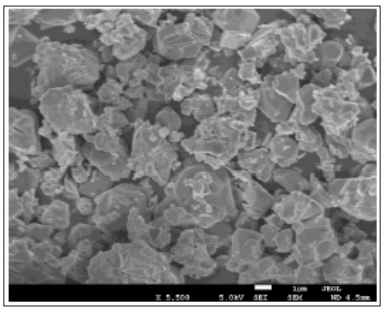

Figure 2 (b): SEM micrographs of $Zn_{0.95}Co_{0.05}O$ samples

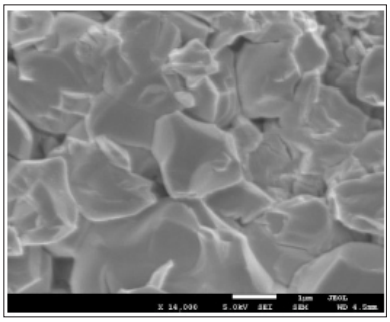

Figure 2 (c): SEM micrographs of $Zn_{0.95}Mn_{0.05}O$ samples

Figure 3(a-c) shows the J-E characteristics for all samples at the considered temperature (300 K, 350 K, 400 K, 450 K and 500 K). It is evident that the behaviour of J-E curves is ohmic in the low field region and non-ohmic in the high field regions. The J-E curves are gradually shifted to lower values of the applied fields as the temperature increases up to 500 K. The upturn region is clearly observed for all samples as the temperature increases up to 400K, and it is completely disappear with further increase of temperature up to 500 K. However, the breakdown field EB is usually taken as the field applied when the current flowing through the varistor is 1 mA/cm^2 [14, 25, 26]. The variation of EB against temperature for all samples is shown in Figure 4 (a). EB is decreased as the temperature increases, and it is between 3.63 V/cm and 2368 V/cm for all samples. The change of EB values with doping it is following the order Mn> Zn > Co.

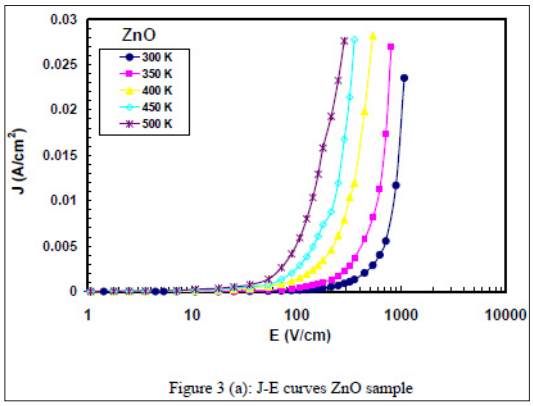

Figure 3 (a): J-E curves ZnO sample

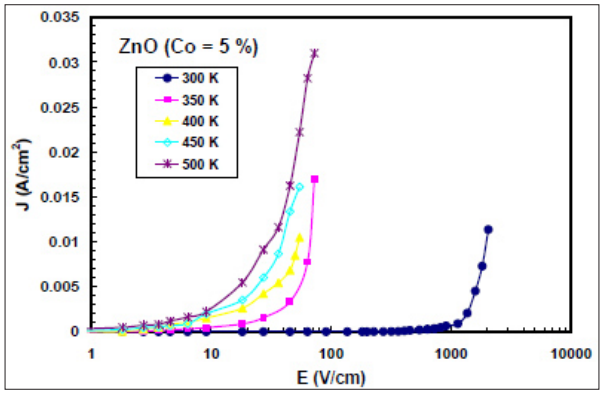

Figure 3 (b): J-E curves $Zn_{0.95}Co_{0.05}O$ sample

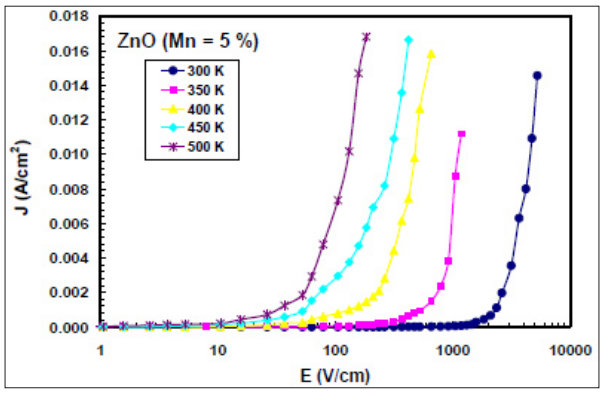

Figure 3 (c): J-E curves $Zn_{0.95}Mn_{0.05}O$ sample

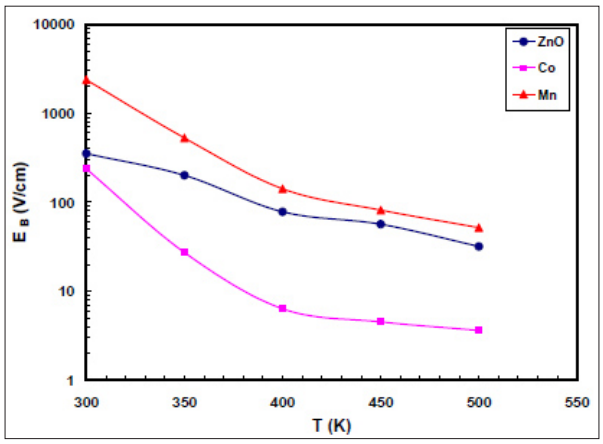

Figure 4 (a): Breakdown field versus temperature for $Zn_{0.95}M_{0.05}$ Samples

The current - voltage relation of a varistor is given by the following equation [25, 26];

$$J = \left(\frac{E}{C}\right)^{\alpha} \qquad (2);$$

Where J is the current density, E is the applied electric field; C is proportionality constant corresponding to the resistance of ohmic resistor (nonlinear resistance) and α is the nonlinear coefficient. The current –voltage curves are plotted on a log-log scale, from which the slope of the curve gives the value of α [9].

The variation of α against temperature in the three different regions is shown in Figure 4 (b). It is apparent that the upturn region is clearly observed by increasing temperature up to 400 K, and it is completely disappear as the temperature increase up to 500 K. The values of α are between 1.65 and 56 for all samples, in the following order Mn > Zn > Co. These results indicate that the increase of temperature up to 400 K deforms the non ohmic features and shifts the breakdown fields to the lower values, as reported [27].

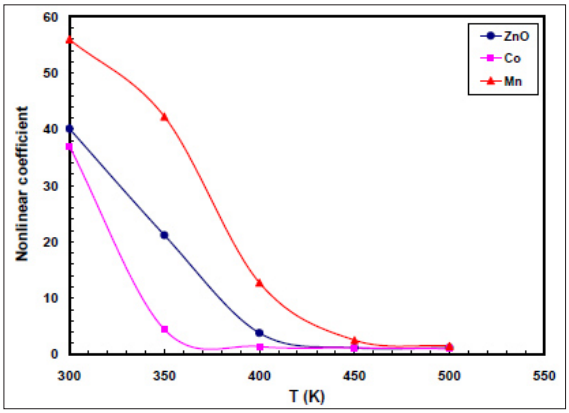

Figure 4 (b): Nonlinear coefficient versus temperature for $Zn_{0.95}M_{0.05}O$ samples

The electrical conductivity against temperature σ for all samples can be calculated from the (J/E) in the linear region, considering the currents and voltages are distributed homogeneously over the cross-section and thickness of the samples. While, in the second region (nonlinear region), the current strongly increase due to the decrease of potential barrier height between the grains φB. Then, the conductivity in the nonlinear region is given by [28];

$$\sigma_2 = \sigma_1 \exp\{\frac{(\alpha-1)(E_2-E_1)}{E_2}\} \quad (3)$$

Where σ1 is the conductivity in the low field region (first region). E1 and E2 are the applied fields across the nonlinear region. In Figure 5 (a-c), we presented the electrical conductivity against temperature through the three different regions for all samples. It is clear that σ is increased by increasing temperature up to 500 K, in the following order Co > Zn >Mn. The lower values of conductivity at low temperature (300 K)

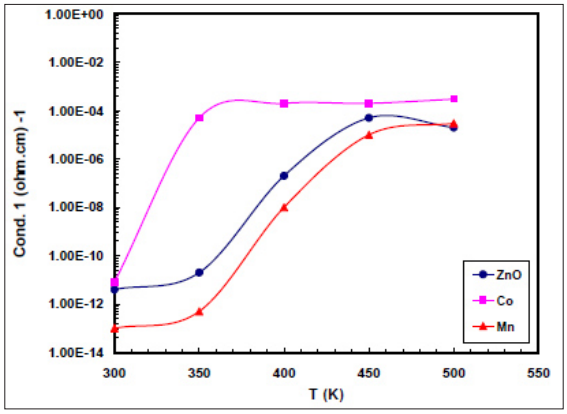

Figure 5 (a): Conductivity 1 versus temperature for $Zn_{0.95}M_{0.05}O$ samples

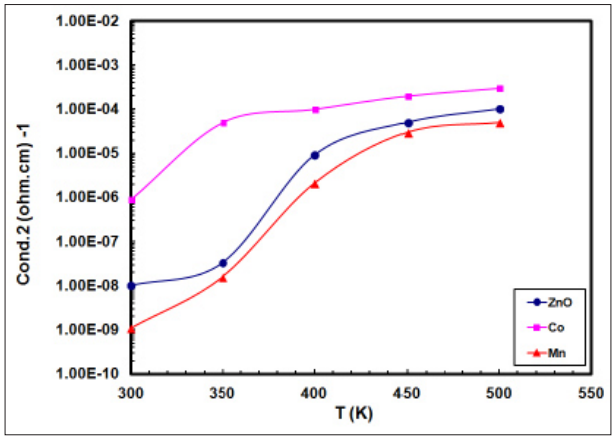

Figure 5 (b): Conductivity 2 versus temperature for $Zn_{0.95}M_{0.05}O$ samples

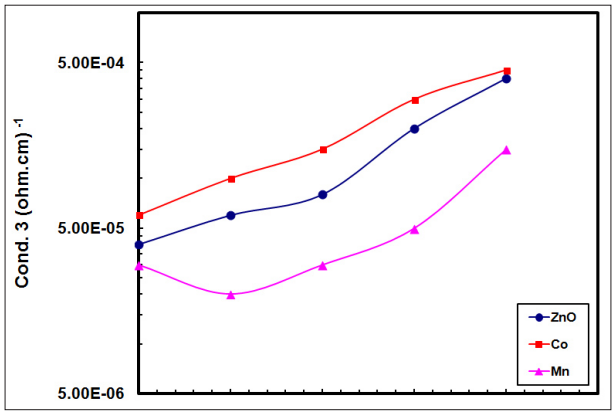

Figure 5 (c): Conductivity 3 versus temperature for $Zn_{0.95}M_{0.05}O$ samples

can be understood as the consequence of the high porosity and small grain size for this type of samples. It is also related to the shape of the intergranular Schottky barrier, which is expected to be wider at low temperature. While, at high temperature up to 500 K, the Schottky barriers is supposed to be thin as a result of electrically active defects produced during heat treatments. In particular, the samples at 300 K show a faster response to the presence of oxygen vacancies, while they show a delay in their response at 500 K. The presence of these vacancies may be originated due to the changes in the height and shape of the barrier and due to adsorption at intergranular regions, which is consistent with the behaviours of breakdown field and nonlinear coefficient against temperature.

However, the conductivity-temperature dependence is found to obey the well-known Arrhenius relation;

$$\sigma = \sigma_0 \exp(\frac{E_a}{K_B T}) \quad (4)$$

Where σ and σ_o are the electrical conductivities at temperatures T and T_o, respectively. E_a is the activation energy over the temperature range. Figure 6 shows the variation of ln σ against temperature as 1000/T. It is clear that the electrical conductivity σ is gradually increased as the temperature increased up to 500 K, in the following order Co > Zn >Mn. Anyhow, we obtained a curvature in the

conductivity curves at 300 K than that of other temperatures. By excluding this point, the activation energy is calculated from the slope of each plot. The different values of Ea are listed inTable 1. The activation energies Eg are 0.194 eV, 0.155 eV and 0.231 eV for all samples, in the following order Zn, Mn and Co.

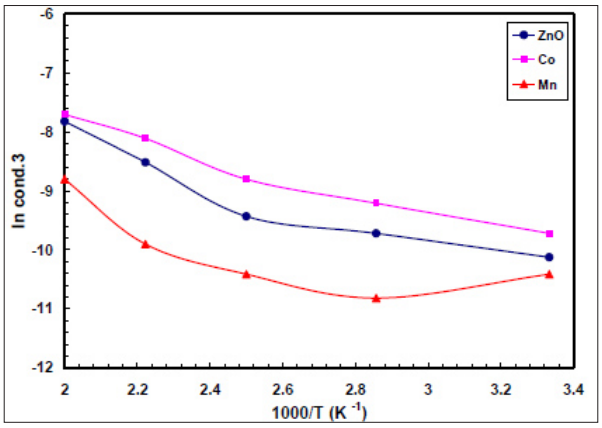

Figure 6: ln σ conductivity versus (1000/T) for $Zn_{0.95}M_{0.05}O$ samples

Anyhow, lot of studies has been done on the effects of 3d transition metal impurities on the electrical conductivity of ZnOvaristor. They investigate that these metals could enhance the excess oxygen concentration in the grain boundary region and a potential barrier is formed preferentially [29-31]. Therefore, the electrical conductivity of doped ZnO samples is apparently lower than that of the ZnO, and the grain boundary is more resistive than the grain. Then the doping can be used in ZnOvaristor to build up the potential barrier in the grain boundary. Now, let us now discuss the effect of the doping individually in place of Zn sites as compared to ZnO.

Table 2: EB and α versus doping content for Zn0.95M0.05O samples

T (K)	EB (V/cm) Zn	EB (V/cm) Co	EB (V/cm) Mn	α Zn	α Co	α Mn
300	351.4	236.4	2368.1	40.1	37	56
350	200.6	27.3	526.3	21.2	4.5	42.3
400	78.1	6.4	141.6	3.82	1.4	12.8
450	56.7	4.6	81.6	1.18	1.2	2.5
500	31.9	3.6	51.8	1.2	1.0	1.5

Mn leads to supporting the formation of the potential barrier in the grain boundaries, and consequently the breakdown field and nonlinear coefficient areimproved. While, the electrical conductivities at room temperature are apparently lower than that of the pure ZnO, indicating that the grain boundary is more resistive than the grains. This is because Zn^{2+} probably nonmagnetic ions, while Mn is magnetic ion with 4.9 μB magnetic moment [16]. Furthermore, the higher valence state of $Mn^{3+/4+}$ as compared to Zn^{2+} led to the formation of acceptor levels and made the grain boundary region more resistive. While with increasing temperature the Mn deep donors may be start to ionize, resulting in an increase of the conductivity. On the other hand, it is found that the Mn-Mn interaction is dominated by anti-ferromagnetic (AFM) coupling from the Curie– Weiss behaviour at high temperature in $Zn^{1-x}Mn_xO$ compounds, and consequently the potential barriers is decreased as compared to RT [32]. But the values of E_B and α against temperature remain higher than that of ZnO. While, the Co^{3+} dopant makes the grains less resistive as compared to ZnO. Above 300 K, Co leads to deformation of the potential barrier formed in ZnOvaristor. While the electrical conductivity is increased, and it is remains higher than of ZnO. However, it has been reported that diluted magnetic semiconductors are formed by partial substitution of n-type ZnO with small amount of magnetic transition metals such as Co^{3+} with 3.5 μB magnetic moment. However, ferromagnetism is considered to originate from the exchange interaction between the free delocalized carriers (holes or electrons from the valence band), and the localized d spins of ions [33, 34- 35].Therefore, the order of ferromagnetism at 300 K produced by Co addition may be the main reason for deformation of barriers of ZnOvaristor, and consequently the electrical conductivity is improved.

However, the d bands result in energy roughly 2 eV too low for activation energy as compared to the experimental value [36-40]. This deviation was attributed to the measured exciton energies influenced by electronic relaxations, which is expected to be mostly pronounced for the highly localized cationic semi-core d states, in consistent with the values of Ea deduced from conductivity curves. However, in Schottky-type barrier, the resistivity is related to electron concentration, n, in the bulk and to the barrier height Φ_B as, $\Phi_B = K(\frac{n}{\Phi_B})^{\frac{1}{2}}$ [34], K is a constant. A diminution in the resistivity could then be ascribed to an increase in the potential barrier height, to a decrease in the donor concentration or eventually, to both phenomena occurring simultaneously. Therefore, the effective activation energy as well as the potential barrier height is raised when the doping is incorporated to the barrier formation at the grain - grain interface. This is consistent with the behaviour of potential barrier for Mn sample rather than that of Zn and Co samples as discussed above. So, the Ea is higher for Mn compared to Zn and Co, as obtained.

Conclusion

Structural and electrical properties of $Zn_{0.95}M_{0.05}O$ ceramic varistors, M = Zn, Co and Mn is reported. We have shown that addition of doping does not influence the hexagonal wurtzite structure of ZnO ceramics. The average crystalline diameters, deduced from XRD analysis are 15 times lower than those obtained from FESEM micrographs. The breakdown field EB is decreased as the temperature increases, in the following order Mn> Zn > Co. The nonlinear region is observed as the temperature increases up to 400 K, and completely disappears at 500 K. Moreover, the electrical conductivity σ is gradually increased as the temperature increases up to 500 K, in the following order Co > Zn >Mn. On the other hand, the activation energies are 0.194, 0.155 and 0.231 eV for all samples, in the following order Mn, Zn and Co. We believe that valence states, magnetic moment and thermo-ionic emission produced by the doping are responsible for the present behaviour.

Acknowledgements

This work was supported in part from research advancement projects no: 140082, King Faisal University, Saudi Arabia. The author thanks the Deanship of Scientific Research, KFU for providing facilities and maintenance support during the present work.

References

1. Joshy Jose, Abdul Khaddar M (2001) Mater SciEng A 810: 304-306
2. Look D C (2001) Mater SciEng B 80: 383.
3. LianGao, Qiang Li , Weiling Luan, HirokazuKawaoka, TohruSekino, et al. (2002) JAm Ceram Soc 85: 1016.
4. Clarke DR (1999) J Am CeramSoc 82: 485.
5. Mukae K, Tsuda K, Nagasawa I (1977) Jpn. J ApplPhys 16:1361
6. Pike GE, Seager CH (1979) JApplPhys 50: 3414.
7. FumiyasuObe, Yukio Sato, Takahisa Yamamoto, Yuichi Ikuhara ,Taketo Sakuma (2003) JAm Ceram Soc 86: 1.
8. Zhen Zhou, Kato K,Komaki T,Yoshino M,Yukawa H, et al. (2004) J Eur Ceram Soc 24:139.
9. Matsouka M (1971) Jpn.J ApplPhys 10: 736.
10. Eda K (1989) IEEE Elect. Insul Mag 5: 28.
11. Han J, Mantas PQ, Senos AMR (2002) J Eur Ceram Soc 22.
12. Look DC, Hemsky JW, SizeloveJR (1999) Phys Rev Lett 82: 2552.
13. Carlson WG, Gupta TK (1982) JApplPhys 53: 5746.
14. Sedky A, Abu-Abdeen M, Abdel- Aziz Al-Mulheim (2007) Physica B 388: 266.
15. Sedky A, AymanSawalha, AmalYaseen (2009) Physica B 404: 3519.
16. Sedky A, El-Suheel E (2010) Physics Research International 1.
17. Glot AB (2006) J Mater Sci Mater electron 17: 755.
18. Senos AMR , Santos MR, Moreira AP , Vieira JM (1988) In surface and Interfaces of Ceramic Materials, ed. Dufour L C, Monty C C , Petot-Ervas G, NATO ASI Series, Kluwer Academic, London 553.
19. Senos AMR , Vieira JM (1993) In Proceedings of the international Conference Third Euro-Ceramics, ed. Duran P, Fernandez J F, Faenza Edit Rice Iberica Faenza SL 1: 821.
20. Senos AMR (1993) PhD Thesis, University of Aveiro, Aveiro.
21. Shan FK, Yu YS (2004) J Eur Ceramic Society 24: 1869.
22. Kisi E, Elcombe MM (1989) ActaCrystallogr Sect C CrystStructCommun C 45: 1867; 30- Guangqing Pei, Changtai Xia, Shixun Cao, Jungang Zhang, Feng Wu,et al. (2006) JMMM 302: 340.
23. Özgür Ü, Ya A, Alivov I, Liu C, Teke A, et al. (2005) J ApplPhys 98: 041301.
24. WurstJC, NelsonJA (1972) Journal of the American Ceramic Society 55: 109-111.
25. Deshpande VV,Patil MM, Ravi V(2006) Ceramic international 32: 85.
26. MouradHouabes, SlavkoBernik, ChabanceTalhi, Ai Bui (2005) Ceramic International 29: 783.
27. Choon -Woo Nahm (2007) Material Science Engineering B 136: 134.
28. Sedky A, MahfozKotb M (2013) Current Applied Physics 13: 2117.
29. Ohashi N, Terada Y, Ohgaki T, Tanaka S, Tsurumi T, et al. (1999) Jpn.J ApplPhys 38: 5028.
30. Oba F, Tanaka I, Adachi H (1999) Jpn.J ApplPhys 38: 3569.
31. Mantas PQ, Baptista IL (1995) JEurCeram Soc 15: 605.
32. Zhao Long, Lu Peng-Fei, Yu Zhong-Yuan, Ma Shi-Jia, Ding Lu, et al. (2012) Chin Phys B 21: 097103.
33. Kittilstved KR, Norberg NS, Gamelin DR (2005) Phys Rev Lett 94: 147209 ; BakhtiarUlHaqa, Afaq A, Ahmed R ,Naseema S (2012) Chin Phys B 21: 097101.
34. AymanSawalha, Sedky A, Abu-Abdeen M (2009) Physica B 404: 1316.
35. Wei SH, Zounger A (1988) Phys Rev B 37: 8958.
36. Guangqing Pei, Changtai Xia, Shixun Cao, Jungang Zhang, Feng Wu, et al. (2006) JMMM 302: 340.
37. Martins JL, Troullier N, Wei SH (1991) Phys Rev B 43: 2213.
38. Xu YN,Ching WY (1993) Phys Rev B 48: 4335.
39. Vogel D, Krüger P, Pollmann J (1995) Phys Rev B 52: R14316.
40. Zakharov O, Rubio A, Blasé X, Cohen ML, Louie SG (1994) PhysRev B 50: 10780.